Nonlinear Evolution of Surface Morphology in InAs/AlAs Superlattices via Surface Diffusion

O. Caha,[1,*] V. Holý,[2] and Kevin E. Bassler[3]

[1]*Institute of Condensed Matter Physics, Masaryk University, Kotlářská 2, 61137 Brno, Czech Republic*
[2]*Department of Electronic Structures, Charles University, Praha, Czech Republic*
[3]*Department of Physics, University of Houston, Houston, Texas 77204-5005, USA*
(Received 11 January 2006; published 6 April 2006)

Continuum simulations of self-organized lateral compositional modulation growth in InAs/AlAs short-period superlattices on InP substrate are presented. The results of the simulations correspond quantitatively to the results of synchrotron x-ray diffraction experiments. The time evolution of the compositional modulation during epitaxial growth can be explained only including a nonlinear dependence of the elastic energy of the growing epitaxial layer on its thickness. From the fit of the experimental data to the growth simulations we have determined the parameters of this nonlinear dependence. It was found that the modulation amplitude does not depend on the values of the surface diffusion constants of particular elements.

The process of self-organization during the growth of semiconductor epitaxial nanostructures is described using two different models [1]. If there is a high density of monolayer steps on the vicinal surface (the crystallographic miscut angle is larger than approximately 1°), a step-bunching instability occurs [2], but if the density of the monolayer steps is low, a self-organized growth of two-dimensional or three-dimensional islands takes place. The latter process occurs if the reduction of the strain energy due to an elastic relaxation of internal stresses in the islands outweighs the corresponding increase of the surface energy [morphological Asaro-Tiller-Grinfeld (ATG) instability [3–5]].

The cited papers analyzed the self-organization process in a linearized approach from which a critical wavelength of the surface corrugation follows as a function of material parameters. The exact nonlinear equation of the surface evolution was studied by Yang and Srolovitz [6] and Spencer and Meiron [7] for the case of a semi-infinite substrate. It was found that the shape of an initially harmonic surface waviness changes and a sequence of deep cusps is created. This behavior was observed using scanning electron microscopy [see, e.g., [8]].

The physical properties of very thin layers (down to few monolayers) differ from the properties of the bulk. This difference leads to the creation of a stable two-dimensional layer at the surface (wetting layer) in the first stage of the Stranski-Krastanov growth mode. The occurrence of this so-called "wetting effect" can be explained by a nonlinear dependence of the elastic energy density on the layer thickness [9,10]. Simulations showed that the wetting-effect suppresses the growth of the cusps and subsequently it leads to the formation of surface islands [11]. These islands are unstable and coalesce [the Ostwald ripening [12]] [13]. However, numerical growth simulations indicate that an anisotropy of the surface energy limits the ripening process and causes the creation of a nearly homo-geneous array of islands [see Ref. [14], among others, and the citations therein].

The evolution of the surface morphology of multilayers has been studied only in a linearized approach so far [15,16]. From this approach, an unlimited growth of the modulation amplitude follows, which does not correspond to the experimentally observed stabilization of the modulation amplitude during the growth. The aim of this Letter is to describe this stabilizing effect using the exact nonlinear equation of growth including the wetting effect. We have simulated the time evolution of the spontaneous lateral modulation of layer thicknesses in short-period semiconductor superlattices and we have found that the evolution of the modulation amplitude quantitatively corresponds to the results obtained by x-ray scattering measurements.

We have studied a series of InAs/AlAs superlattices grown by molecular beam epitaxy on InP (001) substrates. The substrate was covered by a 100 nm thick $In_xAl_{1-x}As$ buffer layer with the same chemical composition as the average composition of the InAs/AlAs stack. The nominal thicknesses of both InAs and AlAs layers were 1.9 monolayers (mL) in all samples. The samples were prepared in a series with 2, 5, 10, and 20 superlattice periods. The growth temperature was 530 °C and the growth rate 0.5 mL/s. The details of the growth can be found elsewhere [17].

X-ray grazing-incidence diffraction (GID) measurements were carried out at beam line ID01 at European Synchrotron Radiation Facility (ESRF) in Grenoble using the x-ray wavelength 1.54 Å. We have measured the diffusely scattered intensity distributions around 400 and 040 reciprocal lattice points in the $q_x q_y$ plane parallel to the sample surface. Two first-order lateral satellite maxima were observed at samples with 5 and more superlattice periods. An example of this experimental intensity map is plotted in Fig. 1. The distance of the lateral satellites from the specular crystal-truncation rod at $q_{x,y} = 0$ is inversely
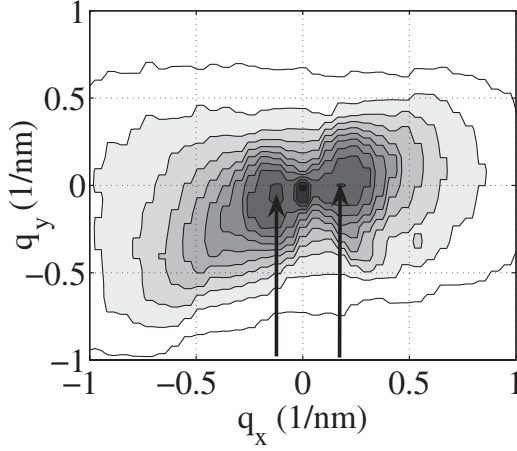
FIG. 1. Diffusely scattered intensity measured around the 400 reciprocal lattice point on the sample with 20 superlattice periods. The contours are logarithmic; four contours correspond to one decade. The diffraction vector is along the q_x axis. The arrows show lateral intensity maxima mentioned in the text.

proportional to the lateral modulation period; the period remains constant for all samples and was determined to be (267 ± 15) Å. From the position of the satellite maxima in the $q_x q_y$ plane we determined the modulation directions close to [310] and [$\bar{1}$30]. The amplitudes of the satellites increase with the growing number of the superlattice periods, while their widths decrease. This indicates that during the epitaxial growth the periodicity of the lateral modulation improves and its amplitude increases. The details of the experimental setup and results are described in the previous paper [18], where we have determined the time dependence of the modulation amplitude from the x-ray data.

The diffuse scattered intensity can be calculated using the formula

$$I_{\text{diff}}(\mathbf{q}) = A \left| \int d^3\mathbf{r} \chi_{\mathbf{h}}(\mathbf{r}) e^{-i\mathbf{h}\cdot\mathbf{u}(\mathbf{r})} \right|^2, \qquad (1)$$

where A is a constant, $\chi_{\mathbf{h}}$ is the crystal polarizability, $\mathbf{h}$ is the diffraction vector, and $\mathbf{u}$ is the displacement vector. Using the procedure described in the previous work [18], we have extracted the correlation function $\varepsilon(\mathbf{x} - \mathbf{x}') = \langle[c(x) - c_0][c(x') - c_0]\rangle$, from the measured data, where $c(x)$ is the local InAs concentration averaged along the growth direction z and c_0 is the average InAs concentration. The dependence of the first coefficient ε_1 of the Fourier series of ε obtained from the experimental data is plotted in Fig. 2; this coefficient corresponds to the modulation amplitude.

The evolution of the surface described by the function $z = h(x, t)$ is driven by the surface diffusion and it can be described by the equation [19]

$$\frac{\partial h(x, t)}{\partial t} = \frac{D_s \theta \Omega}{k_B T} \nabla^2 \mu(x, t) + F + \eta(x, t), \qquad (2)$$
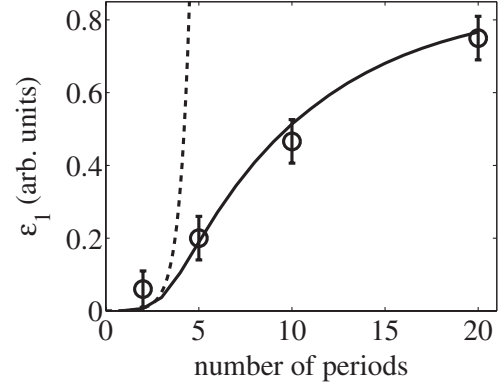
FIG. 2. The dependence of ε_1 on the number of superlattice periods; this dependence describes the time evolution of the modulation during the growth. The circles with error bars are the experimental points obtained from the x-ray data; the full line represents the simulations. The dashed line is the evolution of ε_1 calculated in the linearized case [15,16].

where D_s the surface diffusion coefficient, θ is number of atoms per unit area on the surface, Ω is atomic volume, k_B is the Boltzmann constant, T is the temperature, μ is the chemical potential on the surface, F is the deposition rate, and η is the deposition and diffusion random noise. The model is assumed to be independent on the third coordinate y and hence only one-dimensional surface modulation in a two-dimensional (x, z) space can be simulated. This approach is well justified for quantum wires or for strongly elongated quantum dots. For the quantum dots of a more symmetric shape this simulation can give limited information only. This effect is discussed below.

The chemical potential μ can be expressed as [20]

$$\mu(x, t) = \mu_0 + \gamma\kappa + \frac{1}{2}C_{jklm}\epsilon_{jk}\epsilon_{lm}\bigg|_{z=h(x)} + \frac{df_{\text{el}}^{(0)}(h)}{dh}, \qquad (3)$$

where μ_0 is the chemical potential of an ideally flat unstrained surface, γ is the surface tension, κ is the surface curvature, C_{jklm} are the components of the elastic tensor of the material, and ϵ_{jk} is the strain tensor. The function $f_{\text{el}}^{(0)}(h)$ describes a dependence of the elastic energy density on the layer thickness h giving rise to a wetting effect. For a Ge layer on Si, this function was approximated by the exponential function [20]

$$f_{\text{el}}^{(0)}(h) \approx 0.05 \times E_S[1 - \exp(-h/h_{\text{ml}})], \qquad (4)$$

where E_S is strain energy density in thick flat layer and h_{ml} is thickness of one monolayer. We have used an analogous formula

$$f_{\text{el}}^{(0)}(h) = E_W[1 - \exp(-h/h_W)], \qquad (5)$$

where E_W and h_W are parameters depending on the lattice misfit and elastic constants of the layer.

The strain energy was calculated by a direct solution of the linear elasticity equations using the boundary integral method. The method used is a multiple layer extension of the method in Ref. [6] for an isotropic continuum with periodic boundary conditions. The boundary conditions on the internal interfaces are described in Ref. [21]; the nearly singular integrals were calculated using method developed in Ref. [22].

The simulations have been performed with known material parameters. The surface energy γ, calculated from the first principles, was taken from Ref. [23] as 1 Jm^{-2}. The resulting structure of the interfaces inside the superlattice is shown in Fig. 3. From the simulations, the modulation period of 300 Å follows, which is in a reasonable agreement with the observed value $L_{\exp} = (267 \pm 15)$ Å. It should be noted that the simulated modulation period is affected by the size of the simulated region, since there can be only an integer number of the waves in the simulated system of a given size. To eliminate the influence of the system size we have simulated the growth of several systems of sizes 150, 225, 300, and 400 nm. For various system sizes, the modulation periods were always obtained in the interval (300 ± 20) Å depending on the particular system size. The modulation amplitude is not affected by the system size.

During the growth of first layers in the stack the modulation amplitude grows exponentially as predicted by the linearized theory [15,16]. In the further growth stage, however, the rate of the growth of the modulation amplitude decreases (see Fig. 2, where the experimentally obtained values of the first Fourier coefficient ε_1 of ε are compared with the simulation results).

The simulations show a good agreement with the experimental results in spite of the simplified one-dimensional model of the surface used. Transmission electron microscopy (TEM) on similar samples [17] revealed that the modulation is nearly one-dimensional indeed, resulting in a quasiperiodic sequence of quantum wires;
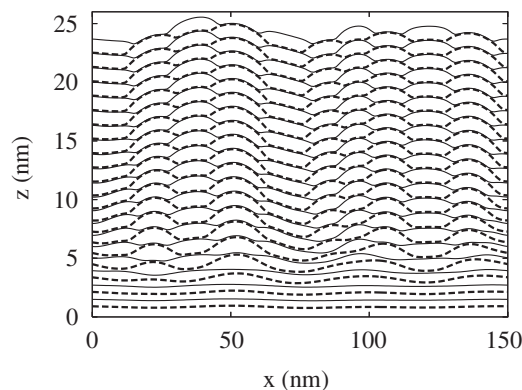
FIG. 3.　Simulated interface profiles in a InAs/AlAs superlattice. Thick dashed lines denote the interfaces between InAs (under) and AlAs (above). Thin solid lines denote the interfaces between AlAs and InAs.

this fact explains why the one-dimensional model is sufficient for the simulation of the modulation kinetics. The TEM observations also demonstrated that if the average lattice parameter of the (relaxed) multilayer is larger than that of the InP buffer underneath (the actual multilayer structure is laterally compressed), the modulation direction is close to [100]; if the multilayer is laterally deformed in tension, the modulation direction is close to the crystallographic directions [310] and [130]. Of course, the one-dimensional model used here cannot predict the modulation direction. We ascribe the dependence of the modulation direction on the deformation sign to the anisotropic surface tension and anisotropy in elastic constants [24]. The degree of anisotropy of the surface tension is also affected by the actual strain in the layer [25] and this fact could therefore also explain different modulation directions in the case of a tensile and compressive deformation of the multilayer.

The continuum simulation also allows for the formation of nonphysical layers, the thickness of which are fractional numbers of monolayers. However, our results based on a continuum approximation are qualitatively similar to the those obtained using an atomistic model and a monolayer step corrugation [2].

The observed and predicted modulation periods roughly correspond to the period given by the linearized theory [15,16], which prediction is $L \approx 200$ Å. According to the Ref. [26] the surface diffusion of In is about 50 times faster than Al, although an exact value of the surface diffusivity of In is not known. In [27] the surface diffusion constant of Al at 530 °C was found to be 1.5×10^{-7} cm^2 s^{-1}. The deposition flux of As atoms is higher than the flux of In and Al atoms at usual MBE conditions [28]; therefore, only diffusivities of Al and In atoms play role.

On the other hand, our simulations have shown that the values of the diffusion constants have nearly no influence on the modulation amplitude, since the diffusion process is sufficiently quick and the growing surface is nearly in an equilibrium state. The diffusion rate, however, affects the modulation *period*. In the case of very slow diffusion (of the order of 10^{-10} cm^2 s^{-1} for Al), the growth of the larger ripples at the expense of smaller ones (the Ostwald ripening) does not take place and the modulation remains constant during the growth of the whole superlattice stack. If the diffusion is very fast (of the order of 10^{-7} cm^2 s^{-1} for Al), the Ostwald ripening takes place during the growth of the first layer already, which leads to the creation of a smaller amount of larger, more distant dots, separated by larger flat areas of a thin wetting layer. The nucleation of the ripples on the subsequent interfaces is affected by the local distribution of lateral strains originated from the large buried ripples. Because of the elastic energy, this distribution gives rise to local minima of the chemical potential at the rims of the buried ripples (two local minima for each ripple) so that the number of the ripples is duplicated. After the deposition of several periods, the ripples cover the

whole interface again and the flat areas between the ripples disappear. The resulting modulation period is approaching the period obtained for a slow diffusion again.

In our simulations, we have achieved a good correspondence of both the modulation period and the time dependence of the modulation amplitude for any value of the diffusion constant of Al between 10^{-10} and 10^{-7} cm^2 s^{-1}.

The resulting interface morphology is substantially affected by the wetting effect, i.e., by a nonlinear dependence of the volume density of the elastic energy on the layer thickness. We have approximated this dependence by Eq. (5). The best correspondence of the measured and simulated modulation amplitudes was obtained for the values $E_W = 0.15 \times E_S$ and $h_W = 0.6 \times h_{\mathrm{ml}}$. We have also estimated these values by means of an atomistic simulation of the elastic energy density using the valence-field force method and the Keating model [29]. In these simulations we have neglected the surface relaxation and reconstruction and we have obtained the dependence of the density of the elastic energy on the thickness of a layer with a flat (001) surface. From the fit of this dependence with exponential formula in Eq. (5) we have obtained $E_W = 0.10 \times E_S$ and $h_W = 0.8 \times h_{\mathrm{ml}}$, which very well corresponds to the values above.

The parameters E_W and h_W affect the modulation amplitude and they have no influence on the modulation period. In the first stage of the multilayer growth the modulation amplitude rapidly increases; this increase is slowed down after the growth of about 10 superlattice periods. The parameter h_W affects mainly the rate of the initial amplitude growth; this rate increases with decreasing h_W. The parameter E_W determines the slowing-down process: for larger values of E_W the slowdown of the amplitude growth is observed earlier than for smaller E_W.

In conclusion, we have simulated the multilayer growth using a nonlinear continuum model. The simulation results agree very well with experimental data obtained by x-ray scattering. From the simulations performed for various values of material parameters we have found that the wetting effect (the nonlinear dependence of the elastic energy density on the layer thickness) has a crucial influence on the resulting interface morphology; from the fit of the experimental data with the simulations we have determined the parameters of this nonlinear dependence and we have compared these values with atomistic simulations.

*Electronic address: caha@physics.muni.cz
[1] J. Stangl, V. Holý, and G. Bauer, Rev. Mod. Phys. **76,** 725 (2004).
[2] L. Bai, J. Tersoff, and F. Liu, Phys. Rev. Lett. **92,** 225503 (2004).
[3] R. J. Asaro and W. A. Tiller, Metall. Trans. **3,** 1789 (1972).
[4] M. A. Grinfeld, Sov. Phys. Dokl. **31,** 831 (1986).
[5] D. J. Srolovitz, Acta Metall. **37,** 621 (1989).
[6] W. H. Yang and D. J. Srolovitz, J. Mech. Phys. Solids **42,** 1551 (1994).
[7] B. J. Spencer and D. I. Meiron, Acta Metall. Mater. **42,** 3629 (1994).
[8] D. E. Jesson, S. J. Pennycook, J.-M. Baribeau, and D. C. Houghton, Scanning Microsc. **8,** 849 (1994).
[9] B. J. Spencer, Phys. Rev. B **59,** 2011 (1999).
[10] J. Tersoff, Phys. Rev. B **43,** R9377 (1991).
[11] T. V. Savina, P. W. Voorhees, and S. H. Davis, J. Appl. Phys. **96,** 3127 (2004).
[12] W. Ostwald, Z. Phys. Chem. (Leipzig) **34,** 495 (1990).
[13] W. Seifert, N. Carlsson, M. Miller, M. E. Pistol, L. Samuelson, and L. R. Wallenberg, Progr. Cryst. Growth Charact. **33,** 423 (1996).
[14] H. R. Eisenberg and D. Kandel, Phys. Rev. B **71,** 115423 (2005).
[15] L. E. Shilkrot, D. J. Srolovitz, and J. Tersoff, Phys. Rev. B **62,** 8397 (2000).
[16] Z. F. Huang and R. C. Desai, Phys. Rev. B **67,** 075416 (2003).
[17] S. P. Ahrenkiel, A. G. Norman, M. M. Al-Jassim, A. Mascarenhas, J. Mirecki-Millunchick, R. D. Twesten, S. R. Lee, D. M. Follstaedt, and E. D. Jones, J. Appl. Phys. **84,** 6088 (1998).
[18] O. Caha, P. Mikulík, J. Novák, V. Holý, S. C. Moss, A. Norman, A. Mascarenhas, J. L. Reno, and B. Krause, Phys. Rev. B **72,** 035313 (2005).
[19] W. W. Mullins, J. Appl. Phys. **28,** 333 (1957).
[20] H. R. Eisenberg and D. Kandel, Phys. Rev. B **66,** 155429 (2002).
[21] J. F. Luo, Y. J. Liu, and E. J. Berger, Comput. Mech. **24,** 448 (2000).
[22] J. F. Luo, Y. J. Liu, and E. J. Berger, Comput. Mech. **22,** 404 (1998).
[23] S. Mirbt, N. Moll, A. Kley, and J. D. Joannopoulos, Surf. Sci. **422,** L177 (1999).
[24] R. F. Sekerka, in *Crystal Growth—From Fundamentals to Technology* (Elsevier, New York, 2004).
[25] V. M. Kaganer and K. H. Ploog, Phys. Rev. B **64,** 205301 (2001).
[26] T. Shitara, D. D. Vvedensky, J. H. Neave, and B. A. Joyce, Mater. Res. Soc. Symp. Proc. **312,** 267 (1993).
[27] M. Kasu and N. Kobayashi, J. Appl. Phys. **78,** 3026 (1995).
[28] M. A. Herman and H. Sitter, *Molecular Beam Epitaxy—Fundamentals and Current Status* (Springer, New York, 1996).
[29] P. N. Keating, Phys. Rev. **145,** 637 (1966).